HGG Advances

ARTICLE

Mosaic variegated aneuploidy syndrome with tetraploid, and predisposition to male infertility triggered by mutant *CEP192*

Jihong Guo,[1,5] Wen-Bin He,[2,3,5] Lei Dai,[4,5] Fen Tian,[1] Zhenqing Luo,[1] Fang Shen,[1] Ming Tu,[1] Yu Zheng,[1] Liu Zhao,[1] Chen Tan,[2,3] Yongteng Guo,[2,3] Lan-Lan Meng,[2,3] Wei Liu,[1] Mei Deng,[1] Xinghan Wu,[1] Yu Peng,[1] Shuju Zhang,[1] Guang-Xiu Lu,[2,3] Ge Lin,[2,3] Hua Wang,[1] Yue-Qiu Tan,[2,3,*] and Yongjia Yang[1,6,*]

Summary

In this study, we report on mosaic variegated aneuploidy (MVA) syndrome with tetraploidy and predisposition to infertility in a family. Sequencing analysis identified that the *CEP192* biallelic variants (c.1912C>T, p.His638Tyr and c.5750A>G, p.Asn1917Ser) segregated with microcephaly, short stature, limb-extremity dysplasia, and reduced testicular size, while *CEP192* monoallelic variants segregated with infertility and/or reduced testicular size in the family. In 1,264 unrelated patients, variant screening for *CEP192* identified a same variant (c.5750A>G, p.Asn1917Ser) and other variants significantly associated with infertility. Two lines of *Cep192* mice model that are equivalent to human variants were generated. Embryos with *Cep192* biallelic variants arrested at E7 because of cell apoptosis mediated by MVA/tetraploidy cell acumination. Mice with heterozygous variants replicated the predisposition to male infertility. Mouse primary embryonic fibroblasts with *Cep192* biallelic variants cultured *in vitro* showed abnormal morphology, mitotic arresting, and disruption of spindle formation. In patient epithelial cells with biallelic variants cultured *in vitro*, the number of cells arrested during the prophase increased because of the failure of spindle formation. Accordingly, we present mutant *CEP192*, which is a link for the MVA syndrome with tetraploidy and the predisposition to male infertility.

Introduction

Correct cell division requires chromosomal duplication and separation into two daughter cells. Errors in this process may result in multipoidy, haploidy, or aneuploidy, which cause human diseases. Mosaic variegated aneuploidy (MVA) syndrome is a rare disorder, in which one-quarter or more of cells in affected individuals have an abnormal number of chromosomes.[1,2] Individuals with MVA syndrome exhibit microcephaly, developmental delay, and other variable abnormalities such as increased risk to malignancies and Dandy-Walker malformation.[2] Several patients with MVA syndrome have been reported in the literature[1–7]; three disease genes have been identified for MVA syndrome, including *BUB1B* (OMIM: 257300),[1] *CEP57* (OMIM: 614114),[6] and *TRIP13* (OMIM: 617598).[7] Tetraploidy is another error in chromosome separation, and it refers to the presence of four copies of the genome in a cell.[8] In humans, tetraploidy has been described frequently in spontaneous abortions[9] and in tumorgenesis.[8] Genetic instability such as MVA is usually preceded by tetraploidy during tumor revolution[9–12] Previously, errors in chromosome segregation have also been reported in male subfertility.[13,14] Variants on a centrosome gene *PLK4*, which controls spindle formation and chromosome separation, has been reported recently on aneuploidy and male infertility.[15–18] Nevertheless, the key molecule that drives the formation of tetraploidy is unknown; not all patients with MVA syndrome can be explained by known MVA genes, and no evidence of a molecule that links MVA, tetraploidy, and infertility together has been reported.

In this study, we report on an interesting family with two siblings who suffer from MVA syndrome with tetraploidy, and other two members who suffer from reduced testicular size and infertility. We show that gene *CEP192* biallelic variants lead to the MVA syndrome plus tetraploidy, and that *CEP192* monoallelic variants lead to predisposition to male infertility by a series of experiments performed on human subjects and mouse models with equivalent variants.

Material and methods

Human subjects

Five members in a family (II-1, II-2, II-5, III-1, and III-2) were recruited from Hunan Children's Hospital. A total of 1,264 idiopathic infertile men with azoospermia, oligozoospermia, and severe oligo-asthenospermia were recruited between June 2017 and

[1]Department of Medical Genetics, Hunan Children's Hospital, Xiangya Medical School & Reproductive Medicine Center, Xiangya Hospital, Central South University, Changsha, China; [2]Hunan Guangxiu Hospital, Hunan Normal University School of Medicine, Changsha, China; [3]Institute of Reproductive and Stem Cell Engineering, NHC Key Laboratory of Human Stem Cell and Reproductive Engineering, School of Basic Medical Science, Central South University, Changsha, China; [4]Department of Obstetrics, Xiangya Hospital of Central South University, Changsha, China
[5]These authors contributed equally
[6]Lead contact
*Correspondence: tanyueqiu@csu.edu.cn (Y.-Q.T.), yongjia727@aliyun.com (Y.Y.)
https://doi.org/10.1016/j.xhgg.2023.100256.

March 2021 in the Reproductive and Genetic Hospital of CITIC-Xiangya, Institute of Reproductive and Stem Cell Engineering, Central South University (Changsha, Human, China). All of them excluded other risk factors of infertility, including chromosomal abnormalities, Y chromosome microdeletion, cryptorchidism, radiotherapy and chemotherapy, infectious diseases, epididymitis, epididymo-orchitis or undescended testis. ES data of such a cohort of patients with idiopathic infertility have been described previously.[19,20] This study was approved by the ethics committee of the Hunan Children's Hospital (for the index family, and for animal experiments, approval number: HCHLL201558, Changsha City, Hunan Province, China) or by Institute of Reproductive and Stem Cell Engineering, Central South University (for 1,264 males with infertility, approval number: LL-SC-2017-025 or LL-SC-2019-034, Changsha City, Hunan Province, China). Appropriate written informed consent was obtained from participating subjects or the guardians of the minors.

G-bands by trypsin using Giemsa (GTG-banding)

The peripheral venous blood of the patients and their family members was collected in a vacutainer sodium heparin vial. Slides were prepared from phytohemagglutinin-stimulated peripheral lymphocyte cultures according to standard cytogenetic methods. In brief, 0.4 mL of whole blood was cultured in lymphocyte medium (5 mL) for 68 h. Then, colchicine (50 μL, 20 μg/mL) was added 2 h before cell harvesting. GTG-banding at a 400–500 band level was performed in accordance with the standard laboratory protocol. Two cultures corresponding to two series of slides from each sample were separately prepared and analyzed. At least 40 metaphases were analyzed for each individual. To confirm that the MVA/tetraploidy/PSCS was not occasional, we performed GTG-banding for several individuals with interests.

Histological analysis

Testes tissues were fixed in Bouin's solution overnight and then embedded into the paraffin. After the tissue blocks were sectioned (5 mm thickness), the tissue slides were generated and deparaffinized by xylene. Then the slides were rehydrated by gradient ethanol, sequentially stained with H&E, and sealed with neutral resin. The images were captured under a microscope (Olympus BX51, Tokyo, Japan).

ES and variant validation

Genomic DNA from peripheral blood samples was extracted using a QIAamp DNA blood midi kit (QIAGEN, Hilden, Germany) according to the manufacturer's protocol. ES was performed on four family members III-1, III-2, II-1, and II-2 (Figure 1A) as described previously.[21,22] Specific PCR primers flanking the suspected variants of *CEP192* were used to amplify the region, including Exon14F: 5′- ttgatgtcatttagctgttttacca-3′; Exon14R: 5′-ccatttaacccctaagttacgc-3′; Exon31F: 5′-gcaatcttattttggaaggcgt-3′; and Exon31R: 5′-cgacacagacacaagtgcat-3′. The purified PCR products were sequenced on a genetic analyzer (Applied Biosystems, CA, A3500). The *CEP192* reference sequence was GenBank: NM_032142.4.

Total RNA preparation and real-time PCR assay

Peripheral blood mononuclear cells (PBMCs) were separated from peripheral venous blood, and then cultured in Gibco RPMI 1640 medium (Thermo Fisher Scientific, 11530586) with phytohemagglutinin stimulation for 48 h. Total RNA was extracted from approximately 1×10^6 PBMCs for each individual by using TRIzol (Thermo Fisher Scientific, 15596026) according to the manufacturer's instructions. First-strand cDNA was synthesized using RevertAid first strand cDNA synthesis kit (Thermo Fisher Scientific, K1622). Real-time PCR was performed using SYBR Green Premix Pro Taq HS qPCR kit (Accurate Biotechnology, China, AG171101) on Roche LightCycler 480 II (Switzerland). The following primers (forward: 5′-GTTGCCTTGGTGGTGGT AAC-3'; reverse: 5′-GTGCCTGGGACTGTTCATTT-3′, predicted size: 186 bp) were used for *CEP192*, and primers (forward:5′-AT GGGGAAGGTGAAGGTCG-3', reverse: 5′-GGGGTCATTGATGG CAACAATA-3′, predicted size: 108 bp) were used for GAPDH (as an internal control). All primers were synthesized by a local biology company (BGI, China).

Minigene analysis

Minigene analysis was performed to investigate whether the c.1912C>T variant of *CEP192* (exon 14) affect the pre-mRNA splicing *in vitro*.[23] Amplified target fragments generated by standard overlapping PCR using the genomic DNA of the II-2 and digestion were cloned into the plasmids vector. The recombinant vectors (WT and MT) were then transiently transfected into MCF-7 and HEK293T cells by using low-toxicity Lipofectamine following the manufacturer's instructions (Life Technologies, Carlsbad, CA). Cells were harvested 48 h after transfection, and total RNA was extracted with TRIzol (Thermo Fisher Scientific, 15596026). Then, cDNA was synthesized by reverse transcriptase using a reverse transcription kit (Thermo Fisher Scientific, K1622) according to the manufacturer's instructions. RT-PCR was performed using specific primers to amplify plasmids containing the exon 14 of *CEP192*. The primers used in the experiments are shown in Table S14. The construction of recombinant plasmids is shown in Figure S10.

Amplicon sequencing

The human c.1912C>T, p. His638Tyr variant was located on exon 14 of *CEP192*. A pair of primers that cover exon 13 and exon 15 was designed (forward: 5′-GTTGCCTTGGTGGTGGTAAC-3′; reverse: 5′-GTGCCTGGGACTGTTCATTT-3′, predicted size: 186 bp). The fragment was amplified using patient cDNA with the predicted size of 186 bp. The PCR product was subsequently sequenced on an Illumina platform (Illumina, San Diego, CA) to detect the frequency of c.1912T transcript.

Generation of *Cep192* mutant mice

Two mouse models were generated on C57BL/6N by CRISPR-Cas9-mediated genome engineering (Cyagen Biosciences, Suzhou, China), including a knockout ($Cep192^{+/-}$) and a knockin ($Cep192^{+/M}$) mice. Exons 6–41 of *Cep192* were deleted from the knockout ($Cep192^{+/-}$) mouse by using the single-guide RNAs (sgRNA-1: GGCGCTGGGCCTCTTTAAAGTGG; sgRNA-2: GGAGA CAAACTCAAGTGACGAGG), which is equivalent to that observed in patients (c.1912C>T). For generating the knockin ($Cep192^{+/M}$) mouse, a single-guide RNA (sgRNA-3: GTTTTTTCTATTCGCA ACACTGG) was designed to target c.5675 A>G/N1892S, which was analogous to the variant p.Asn1917Ser in patients. All experiments involving animals were approved by the institutional animal ethics committee of Hunan Children's Hospital. The strategy and primers sequences used for genotyping the engineered mice are provided in Figures S3 and S4.

In vitro fertilization in mice

In vitro fertilization was conducted in *Cep192* knockout mice, as described previously.[24] In brief, female mice were superovulated via injection with 10 IU of pregnant mare serum gonadotropin, followed by injection of 10 IU of human chorionic gonadotropin (Livzon) 48 h later. After 15–16 h, sperm samples collected from mouse cauda epididymides were added into HTF drop (EasyCheck, M1150). Next, cumulus-intact oocytes collected from superovulated female mice were transferred into a sperm-containing fertilization drop. After incubation for 5 h, mouse embryos were washed in another fertilization drop and transferred into the M16 medium (Sigma-Aldrich, M7292) for further culture (37°C, 5% CO_2). The fertilization rates were evaluated by recording the number of two-cell embryos and blastocysts 20 and 96 h later. For genotyping of blastocysts, whole-genome amplification (WGA) was performed using the REPLI-g single-cell WGA kit (cat. no. 150343), and the following PCR primers and genotyping parameters are provided in Figure S3.

FISH in mice cells

The embryo cells of the *Cep192* mice were analyzed by FISH and compared with a control sample (WT mice in the same litter) using a previously reported method.[25] In brief, the mice embryos were dissected and grinded to single-cell suspension, the suspension was spread on slides, and the cells were fixed, denatured, and hybridized with two specific probes for mouse chromosomes 15 and X (Future Biotech). Subsequently, the slides were rinsed, counterstained, and imaged via fluorescence microscopy.

Immunofluorescence analysis

Cells were plated in gelatin-coated 24-well chamber slides. After 48 h post-plating, the cells were washed with DPBS and fixed for 20 min with 4% paraformaldehyde. After washing, the cells were permeabilized with 0.1% Triton X-100 for 15 min and blocked for 30 min with 5% bovine serum albumin (BSA). Cells were then incubated with first antibodies in 5% BSA at 4°C overnight. Cells were washed several times with PBST. After incubating with secondary antibodies for 1 h, the samples were cover slipped with DAPI. Slides were examined and images were captured under the confocal fluorescence microscopy.

For human cells, rabbit anti-human CEP192 (1:50, Proteintech, 18832-1-AP) and mouse anti-human PCNT (1:100, Abcam, ab28144) were used to analyze the centrosome formation CEP192 co-localization; rabbit anti-human CEP192 and mouse-anti human α-tubulin (1:100, Cell Signaling Technology, no. 3873S) were used to analyze spindle formation. The stage frequency of spindle formation was analyzed by analyzing at least 100 nuclei per slice via randomly selected fields from each slice by two independent researchers who were blinded to the status.

For mouse embryo cells, rabbit anti-mouse CEP152 (1:100, GeneTex, 128027) was used to analyze the centrosome location of a cell. Mouse anti-mouse α-tubulin (1:100, Cell Signaling Technology, no. 3873S) was used to stain microtubules.

TUNEL assay

Terminal deoxynucleotidyl transferase dUTP nick-end labeling (TUNEL) assay (DeadEndTM Fluorometric TUNEL System, Promega, Madison, WI) was performed, according to the manufacturer's instructions, on the cells collected from the Cep192 mutant mice embryos (both the homozygous or heterozygous genotype) and from WT mice embryos (from the same litter).

Mouse embryo cells cultured *in vitro*

E9 embryos (*Cep192*$^{M/M}$, *Cep192*$^{-/-}$, and WT) were used to generate mouse embryonic fibroblasts. In brief, the whole embryo was minced and trypsinized in 0.25% trypsin for 15 min at 37°C. Cells were released through mechanical trituration and grown in Dulbecco's modified Eagle's medium, 10% fetal calf serum, and 100 μg of penicillin-streptomycin per mL.

Human epithelial cells cultured *in vitro*

Sterile urine was collected from the III:2 and an age- and gender-matched control. The outgrowth epithelial cells from urine were collected and seeded onto a gelatin-coated 12-well plate in renal epithelial cell growth medium (REGM BulletKit, Lonza). When epithelial cells were 70%–80% confluent, all cells were subcultured at the next passage with a 1:4 split ratio. During passages 1–3, the epithelial cells were used for the following experiment or frozen in liquid nitrogen for future use. The genotype of cell lines was confirmed by PCR amplification and Sanger sequencing using the primer mentioned above.

Statistical analysis

In the genetic association analysis, two control groups were used, namely, the public Chinese control group (Huabiao-5000 human-exome-sequencing-data of general Chinese-Han-population) and the EAS_gnomAD control group (*CEP192* variants data). Logistic regression analysis was used to estimate the association between a variant (that appears twice or more in 1,264 infertile males) and infertility. Statistical significance was considered when $p < 0.05$. Statistical analyses were conducted using IBM SPSS 20.0 (IBM SPSS, Chicago, IL).

Results

A family with unexplained diseases

III-1 and III-2 (two siblings) experienced microcephaly, developmental delay, limb-extremity dysplasia, facial abnormalities, and reduced testis size came to our clinic for genetic counseling (Figure 1; Table 1; see supplemental note). Patient investigation showed that II-1 and II-5 suffered from reduced testicular volume (Table S1), and that II-5 was completely infertile (Figure 1A). Semen analysis in II-5 revealed severe oligozoospermia (Table S1). Testicular biopsy revealed a comprehensive reduction of germ cells in his available seminiferous tubules without spermatozoa (Figure 1B). Similar semen parameters were observed in II-1 at the age of 47 years (Table S1).

GTG-banding in III-1 and III-2 revealed that 15.52%–24.14% of lymphocytes were tetraploidy cells, 26.44%–27.27% were MVA cells, and 7%–12.33% of metaphase cells showing premature sister chromatid separation (PSCS) (Figures 2 and S1; Table 1; see supplemental note). In addition, a lower but substantial proportion of MVA/tetraploidy cells was observed in II-1, II-2, and II-4 (Table 1; see supplemental note). According to diagnostic criteria

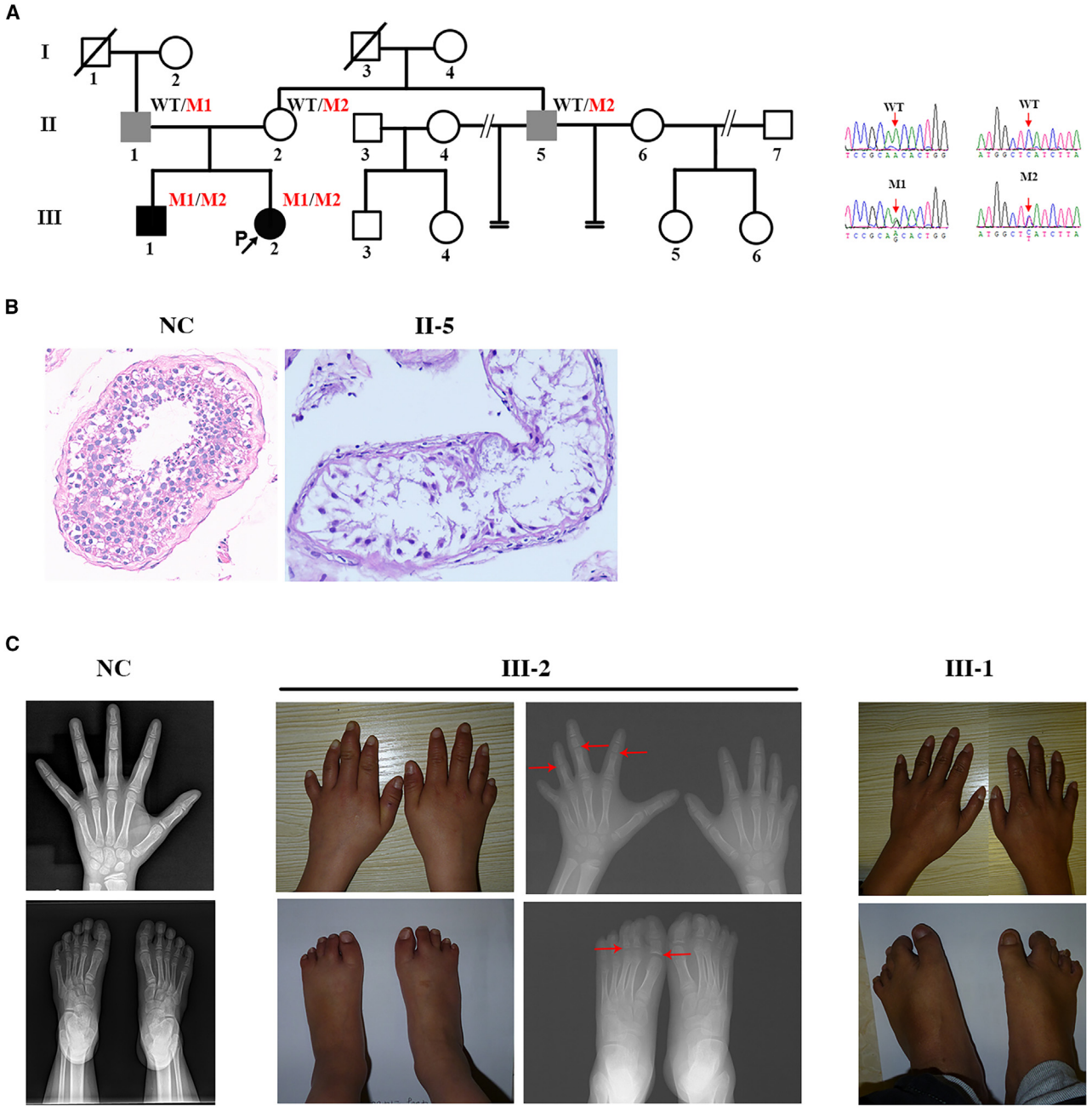

Figure 1. Pedigree, clinical phenotypes, and *CEP192* variants of the family F1

(A) Pedigree and *CEP192* variants validated by Sanger sequencing. Squares and circles denote male and female members. Solid symbols indicate the affected members, and open symbols denote unaffected members. Slashes represent deceased members. Separated double slash, divorce; double horizontal lines, infertility; gray solid symbols, microochidism; black solid symbols, syndromic phenotypes; WT, wild type; M1, variant c.5750A>G, p.Asn1917Ser; M2, variant c.1912C>T, p.His638Tyr; P, proband.

(B) Histological analyses of testicular tissues by H&E staining. Left: representative normal control tubule from a 59-year-old man with prostate cancer. Right: representative tubule of II-5 at age 39 years.

(C) Limb extremities malformations identified by X-ray images. NC, an 8.7-year-old healthy girl. III-1 and III-2 have similar malformations in fingers and toes. Fingers: brachydactyly, dysplasia in middle and distal phalanges, lack of middle phalanges of little finger, absent epiphyseal ossification centers in the 2nd–4th middle phalanges (arrow). Toes: lack of middle phalanges of the 2nd–5th toes, syndactyly of the 2nd and 3nd toes (webbed toes), syndactyly of the 4th and 5th toes (webbed toes), absent epiphyseal ossification centers in the proximal phalanges of the great toe and from the 2nd to 4th toes (arrow).

(a quarter or more cells were MVA),[1,2] III-1 and III-2 fulfilled the diagnosis of MVA syndrome. Considering that, in addition to MVA, III-1 and III-2 also had tetraploidy, and tetraploidy has never been described in patients with MVA syndrome. Accordingly, we propose a subtype of MVA syndrome, namely, the MVA syndrome with tetraploidy, for the siblings. To search for the cause for the family, we performed variant screening for known MVA

Table 1. Cytogenetic phenotypes of the affected individuals with *CEP192* variants

ID	*CEP192* variants	Cytogenetic phenotypes
F1: III-1	biallelic: c.1912C>T, p.His638Tyr c.5750A>G, p.Asn1917Ser	87 cells analyzed 23 cells (26%) were MVA 21 cells (24%) were tetraploidy
F1: III-2	biallelic: c.1912C>T, p.His638Tyr c.5750A>G, p.Asn1917Ser	121 cells analyzed 33 cells (27%) were MVA 29 cells (24%) were tetraploidy
F1: II-1	monoallelic: c.5750A>G, p.Asn1917Ser	106 cells analyzed 14 cells (13%) were MVA 3 cells (3%)were tetraploidy
F1: II-2	monoallelic: c.1912C>T, p.His638Tyr	106 cells analyzed 15 cells (14%)were MVA 2 cells (2%)were tetraploidy
F1: II-4	monoallelic: c.1912C>T, p.His638Tyr	64 cells analyzed 8 cells (13%) were MVA 2 cells (3%) were tetraploidy
Y8147	monoallelic: c.5750A>G, p.Asn1917Ser	286 cells analyzed 34 cells (12%) were MVA 2 cell (1%) was tetraploidy
Y8147 (mother)	monoallelic: c.5750A>G, p.Asn1917Ser	104 cells analyzed 21 cells (20%) were MVA 1 cell (1%) was tetraploidy
T00643	monoallelic: c.5750A>G, p.Asn1917Ser	77 cells analyzed 12 cells (16%) were MVA 1 cell (1%) was tetraploidy
MD3337	monoallelic: c.5750A>G, p.Asn1917Ser	N/A

F1, the index family; MVA, mosaic variegated aneuploidy. N/A, not available.

syndrome genes (e.g., *BUB1B*, *CEP57*, and *TRIP13*),[1,6,7] but no causative variant was identified.

Identification of *CEP192* variants

Exome sequencing (ES) was successfully performed for II-1, II-2, III-1, and III-2 (Table S2). Considering that MVA syndrome is a rare, autosomal recessive disorder,[1,6,7] we focused on genes with rare biallelic variants in III-1 and III-2 according to reasonable filtering strategy (Figure S2). Only two compound heterozygous variants of *CEP192* (NM_032142.4; c.1912C>T, p.His638Tyr and c.5750A>G, p.Asn1917Ser) met the filtering criteria. Sanger sequencing identified that the *CEP192* biallelic variants were co-segregated with syndromic phenotypes in III-1 and III-2, and that the *CEP192* monoallelic variant was co-segregated with reduced testicular-size/infertility in II-1 and II-5 (Figure 1A).

CEP192 associated with male infertility in the general population

We determined whether *CEP192* variants were involved in male infertility in general population. Variant screening of the *CEP192* coding regions was performed for 1,264 unrelated males with idiopathic infertility. By focusing on rare variants (MaF < 0.001 in Eas_gnomAD), 83 variants were retained (Table S3). The p.Asn1917Ser variant of *CEP192* was recurrently detected in three unrelated infertile males with reduced testicular volumes (Y8147, T00643, and MD3337; Table 1). In addition, other variants on *CEP192* were repeatedly detected in infertile males (Tables S4–S6). Results of logistic regression showed that the c.5750A>G, p.Asn1917Ser of *CEP192* was significantly associated with increased risk of infertility (OR = 15.707; 95% CI, 1.76–140.59; p = 0.001; Table S4). Clinical reevaluation confirmed that all three males with p.Asn1917Ser variant were infertile, and GTG-banding results revealed that a substantial part of the cells was MVA/tetraploidy (Table 1; see supplemental note).

Evolutionary conservation of p.Asn1917, and abnormal splicing of c.1912C>T

CEP192 is a 2,537-residue-long protein with 8 tandem domains in its C-terminal part that are similar to members of the PapD-like superfamily.[26] Tandem domains 4 and 5 of human CEP192 constitute the Spd2 domain, which is ubiquitously present in all SPD2/CEP192 homologs and represents the most conserved region among the protein.[26,27] The p.Asn1917Ser variant is located in tandem domain 5 (Figure 3A). However, the other variant, namely, the c.1912C>T, p.His638Tyr, is located on the N-terminal, which is not conserved among different species (Figure 3A). The "Y" amino acid can be seen in residue 638 in *Nannospalax galili* (Figure 3A). However, *in silico* prediction[28,29] estimated the c.1912C>T variant effects of normal splicing by disrupting exon 14 donor splice site. Total RNA was then extracted from patient cells, and a complementary strand of DNA (cDNA) was generated. qPCR assay showed that *CEP192* cDNA was considerably

Figure 2. Representative metaphase cells of mosaic variegated aneuploidy and tetraploidy identified in lymphocytes of III-1 and III-2 of family F1

Note: original figures are shown in Figure S1.

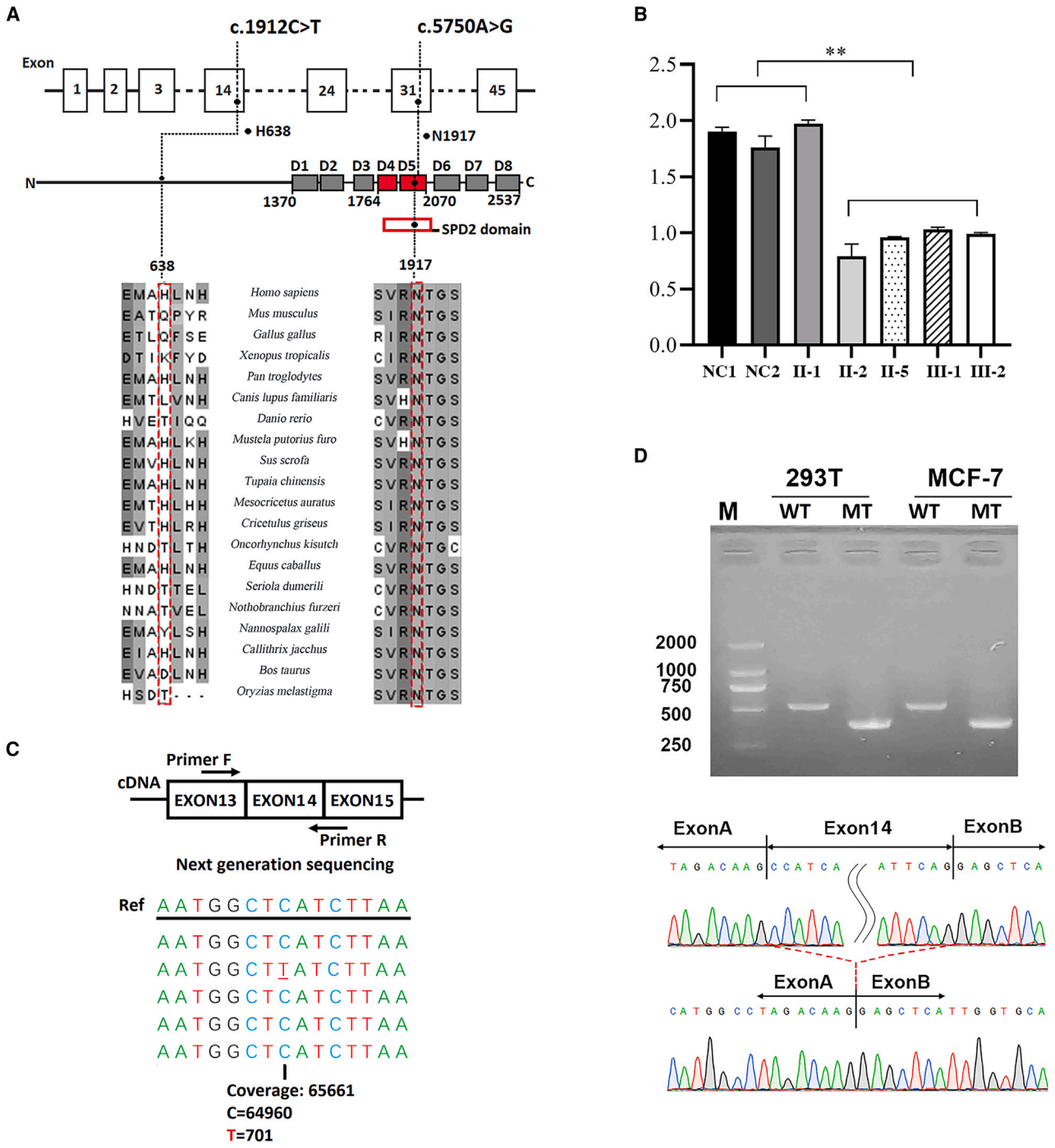

Figure 3. Functional evaluation of *CEP192* variants

(A) Location of two variants (c.1912C>T, p.His638Tyr and c.5750A>G, p.Asn1917Ser) in the *CEP192* gene (upper) and in the known domains of protein (middle). Sequence alignment of CEP192 residue 638 and residue 1,917 across different species (bottom). Note: H638, p.His638; N1917, p.Asn1917.

(B) Expression level of *CEP192* mRNA in individuals with or without c.1912C>T variant. The relative abundance of *CEP192* mRNA expression was calculated by normalization to ACTB level.

Group 1: individuals NC1, NC2, and II-1 without *CEP192* c.1912C>T. Note: NC1 and NC2 were two unrelated healthy individuals, II-1 was a family member with c.5750A>G but without c.1912C>T. Group 2: individuals II-2, II-5, III-1, and III-2 with *CEP192* c.1912C>T variant. The statistical significance of the departure of the observed ratio from the expected ratio is represented by **$p < 0.01$.

(C) Composition analysis of c.1912C>T transcripts in lymphocyte cells of II-2 by next-generation sequencing.

(D) Minigene assay for c.1912C>T variant of *CEP192*.

Upper: PCR products amplified from RT-PCR products (from HEK293T and MCF-7 cells, respectively) were separated by electrophoresis. An approximately 500 bp fragment was identified in the pcMINI-CEP192-WT cells, and a small fragment was identified in pcMINI-CEP192-MT cells (in both HEK293T or MCF-7 cells). Bottom: Sanger sequencing of the RT-PCR products illustrated the skipping of exon 14 (whole exon 14, 127 bp) in mutant status. WT, wild type; MT, *CEP192*, c.1912C>T variant; M, ladder.

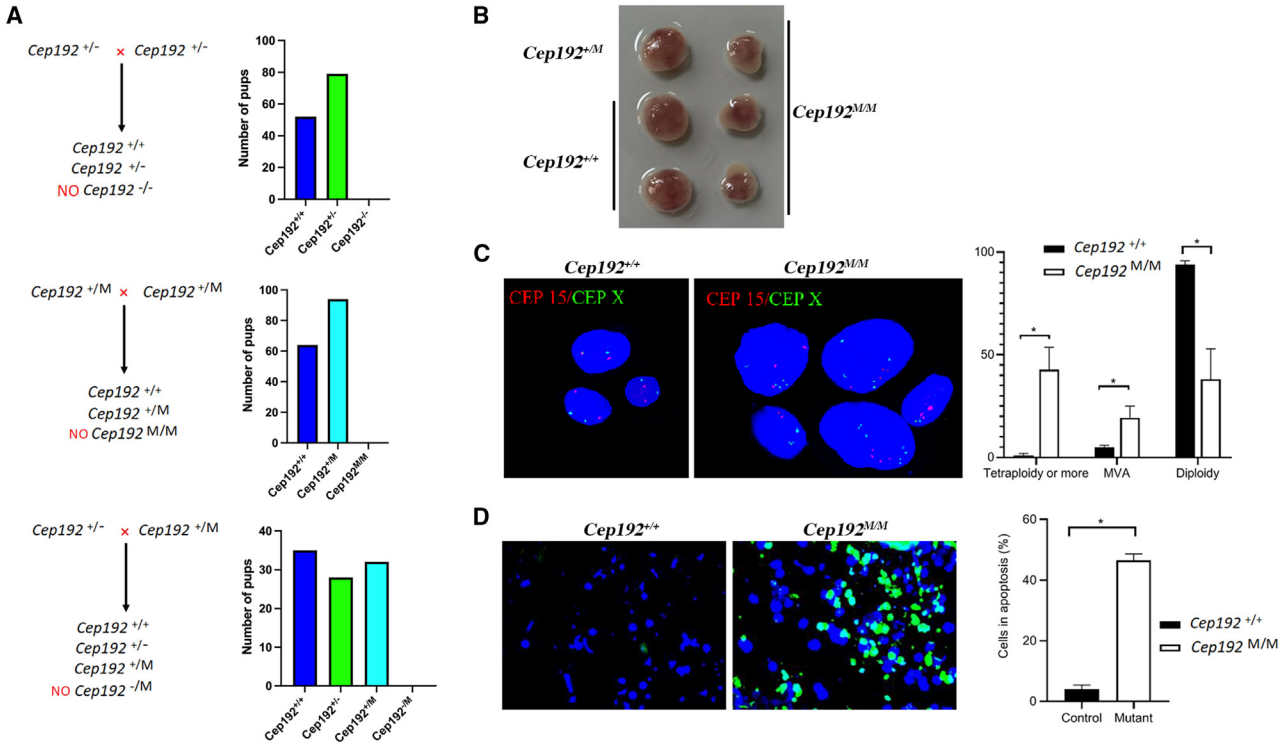

Figure 4. Genetic analysis performed on mouse models

(A) Genotype analysis of progeny from the heterozygous intercrosses.

(B) Representative embryos with different genotypes in E10. *Cep192*$^{M/M}$ embryos arrested at about E7.

(C) Representative interphase nuclei monitored by fluorescence *in situ* hybridization. Left: cells from wild-type embryos, three cell nuclei stained by two red (chromosome 15) and two green (chromosome X) signals. Middle: cells from mutant embryos (upper left, three red and five green signals; upper right, five green and four red signals; lower left, two green and two red signals; lower middle, four green and four red signals; lower right, three red and two green signals). Right: count of normal diploidy cells, MVA, and tetraploidy cells for *Cep192* mutant or wild-type embryo cells. For each sample, randomly 100 cells were analyzed (n = 3). The statistical significance of the departure of the observed ratio from the expected ratio is represented by *$p < 0.05$.

(D) Apoptosis (cells stained by green) in cells from wild-type or *Cep192*$^{M/M}$ stagnated embryos (n = 3). The statistical significance of the departure of the observed ratio from the expected ratio is represented by *$p < 0.05$.

reduced in cases with c.1912C>T compared with that without the c.1912C>T variant (Figure 3B). The *CEP192* transcript at the mRNA level was assessed by next-generation sequencing on a member with heterozygous c.1912C>T variant. Results showed that the c.1912T transcripts were detected in approximately 1% of the overall reads (Figure 3C). Furthermore, mini-gene assay showed that c.1912C>T led to the skipping of exon 14 (Figure 3D), resulting in a frameshift and a premature termination codon p.Pro604Glu*2. Thus, the functional mechanism of c.1912C>T should be the vast majority of mutant transcripts undergoing abnormal splicing, and the shortened transcripts mediated nonsense-mediated mRNA decay.

Animal models confirmed that both *CEP192* variants are pathogenic

Two lines of *Cep192*-edited mice were generated consisting of a knockin mouse (*Cep192*$^{+/M}$) with a variant equivalent to human p.Asn1917Ser and a knockout mouse (*Cep192*$^{+/-}$) mimicking the haploinsufficiency effect of the human c.1912C>T splicing variant (Figures S3 and S4). In progeny derived from the crosses between two *Cep192*$^{+/-}$ mice, the ratio of *Cep192*$^{+/+}$ to heterozygote (*Cep192*$^{+/-}$) was close to 1:2 (34 litters, 131 offspring calculated, *Cep192*$^{+/+}$ = 52, *Cep192*$^{+/-}$ = 79). No *Cep192*$^{-/-}$ offspring was obtained (Figure 4A; Table S7), suggesting embryonic lethality in the *Cep192*$^{-/-}$ state. In parallel, in the progeny derived from the crosses between two *Cep192*$^{+/M}$ mice, the ratio of *Cep192*$^{+/+}$ progeny to *Cep192*$^{+/M}$ was close to 1:2 (21 litters, 158 offspring calculated, *Cep192*$^{+/+}$ = 64, *Cep192*$^{+/M}$ = 94). No *Cep192*$^{M/M}$ offspring was obtained (Figure 4A; Table S8). Subsequently, *Cep192*$^{+/M}$ mice were bred with *Cep192*$^{+/-}$ mice to further verify the causality of both variants. The *Cep192*$^{+/+}$, *Cep192*$^{+/-}$, and *Cep192*$^{+/M}$ progeny can be survivable. However, no *Cep192*$^{-/M}$ mice were obtained (Figure 4A; Table S9). The above results implicated that both the knockout and the p.Asn1917Ser allele were causative agents.

Mutant mice replicated MVA and tetraploidy phenotypes

In vitro fertilization was performed. *Cep192* homozygous mutant embryos could develop into blastocysts *in vitro*

(Figure S5). To explore the stage(s) in which the homozygous embryos undergo arrestation, we sacrificed pregnant mice at various days post coitum. Embryos were dissected at various developmental stages. *Cep192*$^{-/-}$ embryos appeared morphologically normal at E7 compared with their *Cep192*$^{+/-}$ or *Cep192*$^{+/+}$ littermates (Figure S6). Embryonic death was detected for *Cep192*$^{M/M}$ embryos at E10, the size of dead embryos is equivalent to that in E7 (Figure 4B). The same results were observed on *Cep192*$^{-/-}$ embryos (Figure S7). Embryos were dissected and ground to cell suspensions. Fluorescence *in situ* hybridization (FISH) showed a significant increase of MVA and tetraploidy cells in *Cep192*$^{M/M}$ embryo cells (Figure 4C). TUNNEL assay revealed that the number of apoptotic cells increased in *Cep192*$^{M/M}$ embryos compared with that of *Cep192*$^{+/+}$ embryos (Figure 4D). Similar results were obtained in cell samples from *Cep192*$^{-/-}$ embryos (data not shown).

In addition, when *Cep192*$^{+/-}$or *Cep192*$^{+/M}$ males were mated with wild-type (WT) females, approximately 10% of the mated females experienced dystocia. The uteri of females with dystocia were dissected. Fetuses arrested in about E13–E14 were observed; all arresting fetuses were heterozygous (23 tested, 10 were *Cep192*$^{+/-}$; 13 were *Cep192*$^{+/M}$) (Figure S8). Similar to *Cep192*$^{-/-}$ or *Cep192*$^{M/M}$ dead embryos, a remarkable proportion of cells (from the *Cep192*$^{+/-}$ or *Cep192*$^{+/M}$ arrested embryos) were MVA or tetraploidy (Figure S9). TUNNEL assay also revealed that up to 40%–50% of the cells from the *Cep192*$^{+/M}$ arrested embryos underwent apoptosis (Figure S9).

Male mice with *Cep192* heterozygous variants replicated infertility

Breeding assays were performed to check the reproductive capability of male mice with *Cep192* heterozygous variants. *Cep192*$^{+/-}$ males were mated with WT females from complete sexual maturity (2 months) to 9 months. In comparison with WT males mated with WT females with average number of litters of 6.6, the *Cep192*$^{+/-}$ or *Cep192*$^{M/-}$ males mated to WT females exhibited reproductive defects with phenotypic variation among individuals (Figure 5; Tables S10–S12). The number of litters or pups was reduced considerably in *Cep192*$^{+/-}$ or *Cep192*$^{+/M}$ males when they mated with WT females (Figures 5A and 5B; Tables S10–S12). Histological analysis was performed. In the majority of the fertile heterozygotes, testicular size and histology appeared normal. However, the testes of the infertile *Cep192*$^{+/-}$ or *Cep192*$^{+/M}$ males were smaller than those of the *Cep192*$^{+/+}$ littermates (Figures 5C and 5D; Table S13). Hematoxylin and eosin (H&E) staining revealed that, in comparison with a large number of sperms shown in the epididymides of Cep192$^{+/+}$males, the epididymides of the infertile heterozygous mice were nearly empty (Figure 5E). Meanwhile, in comparison with Cep192$^{+/+}$ littermates, a substantiate reduction of germ cells was observed in the seminiferous tubules of infertile Cep192$^{+/-}$ or Cep192$^{+/M}$ males (Figure 5E).

Spindle formation was disrupted in *CEP192* mutant cells

Mice embryo cells were cultured *in vitro*. Only a few *Cep192*$^{-/-}$ or *Cep192*$^{M/M}$ cells can adhere to disk walls (less than 1% vs. *Cep192*$^{+/+}$ 60%). For the cells that can adhere, the cell division was very slow (almost cannot divide). As shown in cells in the interphase, the mutant cells exhibited bipolarized (or dysmorphic) cell shape (Figure 6). In comparison with *Cep192*$^{+/+}$ cells, an appropriate number of microtubules (MTs) were arranged in an orderly manner around the centrosome, the *Cep192*$^{-/-}$ or *Cep192*$^{M/M}$ cells exhibited decreased volume of MTs, and the MTs were disorganized (Figures 6A and 6B). Some of the mutant cells seem to lack a microtubule organizing center (MTOC) (Figures 6A and 6B). In several cells likely in mitosis, chromosomes arranged around lacking a spindle formation (Figure 6B). The investigation was focused on human cells with *CEP192* variants to check the spindle status in mitotic cells. Epithelial cells (from III-2) were cultured *in vitro*. In the prophase, the nucleation of MTs occurred randomly, leading to disorganized, non-bipolar structures of spindle structure (Figure 7). Quantitative analysis was performed and indicated that the *CEP192*-mutated cells exhibited an increased proportion of mitotic cells in prophase (81.90% vs. 20.38% in control cells, Figures 7E and 7F). We propose here that cells lacking normal spindle structure have high probability to be developed to the MVA or tetraploidy cells.

Discussion

In this study, we investigated a family with two siblings who suffered from developmental delay, microcephaly, limb extremities malformation, and reduced testicular size. In addition, two other male family members showed reduced testicular size/infertility. Genetic inheritance was initially unknown for the family. The performance of GTG-banding identified MVA and tetraploidy cells in the patients. ES and further validation disclosed that *CEP192* biallelic variants associated with the MVA syndrome with tetraploidy, and the *CEP192* mono-allelic variants associated with reduced testicular size/infertility. From 1,264 unrelated patients, the same heterozygous *CEP192* variant (in family F1) and other variants were associated with male infertility, confirming that *CEP192* is involved in male infertility. Accordingly, two mice models with equivalent variants were generated. Mutant mice replicated MVA/tetraploidy cytogenetic phenotypes. Patient II-5 and the infertile heterozygous mice (*Cep192*$^{+/-}$, Cep192$^{+/M}$) presented with spermatogenic failure. The patient suffered from Sertoli cell-only syndrome, and the testicular tissue of infertile heterozygous mice showed significant decreased spermatocytes and severe oligozoospermia. This may be due to the species differences between mice and humans. In Online Mendelian Inheritance in Man (616426), *CEP192* is a protein-coding gene without a clear link to human disease. Thus, this study should represent the identification of *CEP192* that links to two human

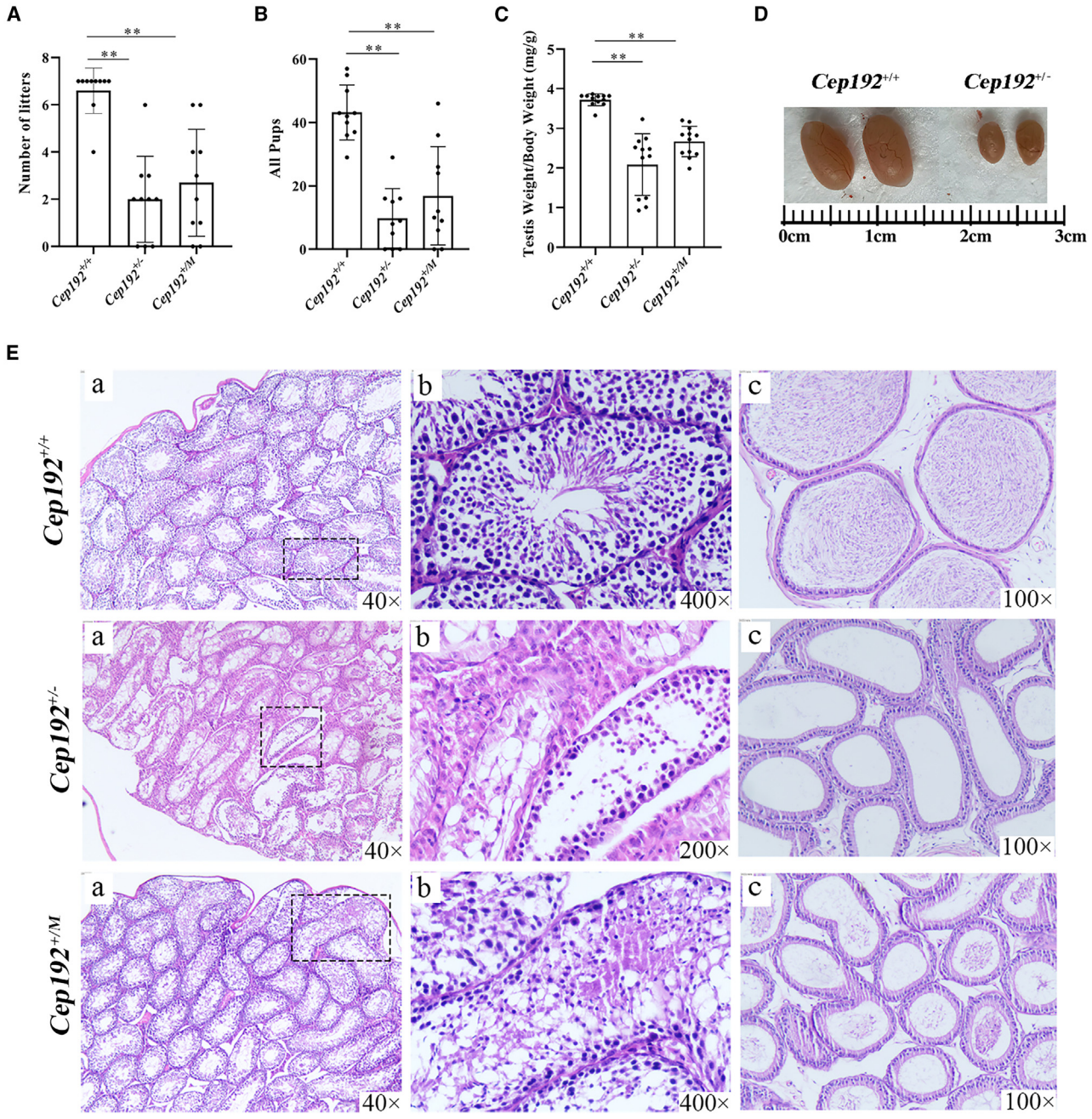

Figure 5. Reproductive phenotypes of infertile male mice with *Cep192* heterozygous variant

(A and B) Number of litters and total pups from the persistent mating of $Cep192^{+/-}$, $Cep192^{+/M}$, or wild-type males with wild-type females from complete sexual maturity (2 months) to 9 months. **$p < 0.05$.

(C) Testes to body weight ratios of infertile heterozygous mice ($Cep192^{+/-}$, $Cep192^{+/M}$) and wild-type mice at 180 days. **$p < 0.05$.

(D) Representative figure of testes between a $Cep192^{+/-}$ mice with infertility and a wild-type mouse at 180 days.

(E) H&E staining of testes (a and b) and epididymides cauda (c) from wild-type mice and infertile heterozygous mice ($Cep192^{+/-}$, $Cep192^{+/M}$) at 180 days.

diseases, the MVA syndrome with tetraploidy and male infertility.

CEP192 encodes a centrosome protein. Centrosomes are organelles that serve as the MTOC for animal cells.[30–32] Experiments *in vitro* by RNA interference indicated that, in the M phase, CEP192 is important for spindle formation[30]; in the interphase, CEP192 plays an important role in MT organization (when it depleted, cells became "slim shape").[33] In this study, by focusing on MVA/tetraploidy cellular phenotypes, we identified *CEP192* natural variants associated with human disorders. The molecular mechanisms behind the formation of tetraploidy here is probably the failure of cell division after chromosome replication due to absence of functional CEP192. Based on the cells from both human and mice, cells in M phase with *CEP192* biallelic variants exhibited disorganized,

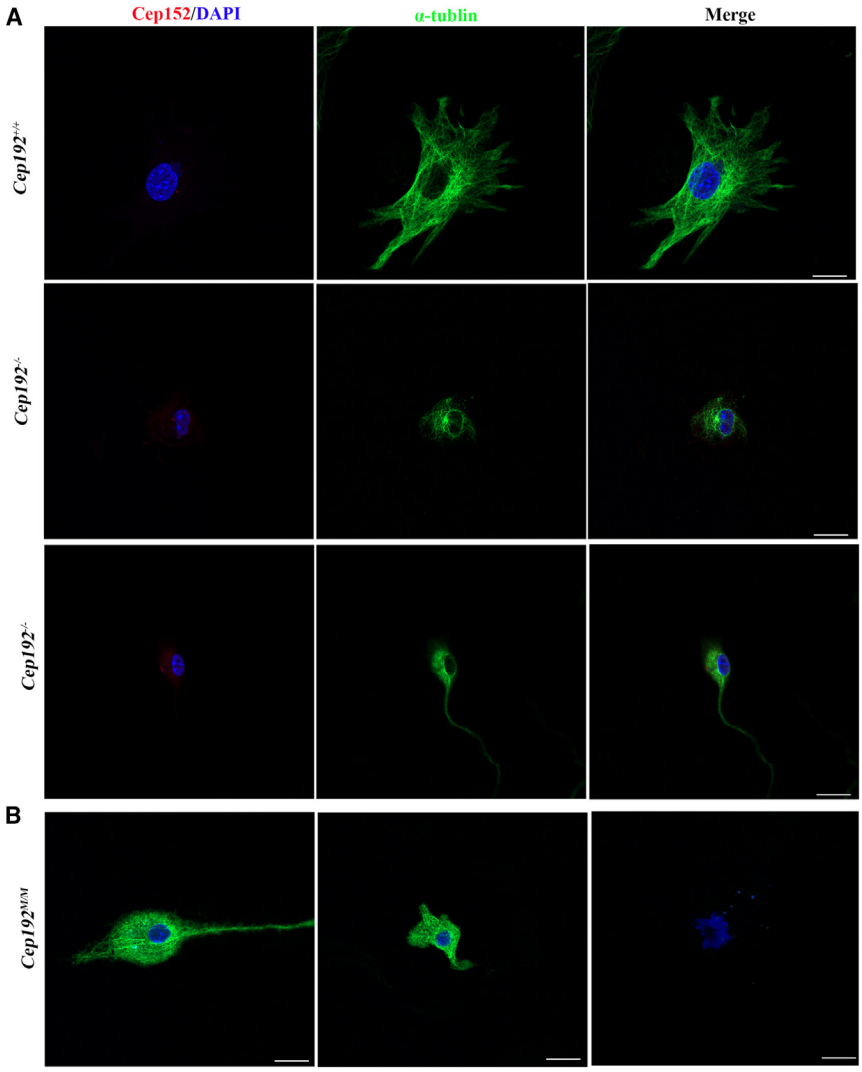

Figure 6. Alteration in mouse primary embryonic fibroblasts without functional CEP192

(A) Immunofluorescence staining of primary embryonic fibroblasts from wild-type (*Cep192*$^{+/+}$) and knockout (*Cep192*$^{-/-}$) mice by using antibodies against a centrosome marker protein CEP152 (red), microtubules (green), and DAPI staining of DNA (blue). Top: CEP152 was co-localized with the microtubule organizing center (MTOC) in *Cep192*$^{+/+}$ cell. Middle: one CEP152 signal was co-localized with MTOC in the *Cep192*$^{-/-}$cell, but the other mutant was not. Bottom: two CEP152 signals were located in cytoplasm distal to the nuclear (obviously not in MTOC) and a CEP152 signal in MTOC in a unipolarized cell. Scale bars, 7.5 μm.

(B) Immunofluorescence staining of primary embryonic fibroblasts from knockin (*Cep192*$^{M/M}$) mice by using antibodies against microtubules (green) and DAPI staining of DNA (blue). Left: a bipolar cell. Center: an abnormal multipolar cell. Right: cell in mitosis but without spindle and without microtubule. Scale bars, 7.5 μm.

non-bipolar structures of the spindles; in the interphase, mice fibroblasts with biallelic variants exhibited an elongated, bipolar, unipolar, or multipolar cellular shape. Therefore, this study proved that CEP192 was vital for spindle formation (in mitosis) and normal MT organization (in interphase) from a new perspective.

Notably, different embryonic development fate was observed between humans and mice with *CEP192* biallelic variants. Mouse embryos with biallelic *Cep192* variants (*Cep192*$^{M/M}$ *Cep192*$^{M/-}$ *Cep192*$^{-/-}$) were arrested at about E7, whereas humans with *CEP192* compound heterozygous variants (c.1912C>T, p.His638Tyr and c.5750A>G, p.Asn1917Ser, i.e., the III-1 and III-2) were survivable. Such a situation may result in subtle differences in one of variants between humans and mice. *Cep192*$^{M/M}$ mice variant c.5675 A>G, p.AsnN1892Ser was equivalent to human c.5750A>G, p.Asn1917Ser variant, while the *Cep192*$^{-/-}$ mice genotype (complete knockout) was different from human c.1912C>T, p.His638Tyr. In mouse model generation, considering that c.1912C>T, p.His638 (human) is not conserved among different species, but the major portion of c.1912T transcripts was undetectable in patient RNA sequencing (as abnormal spicing), *cep192* knockout mice were generated to mimic the effects of the c.1912C>T, p.His638Tyr variant. However, unlike the complete knockout in mice, approximately 1% of c.1912T transcripts can be detected in patient cells (Figure 3C). Therefore, approximately 1% of the c.1912T transcripts (those escaping exon 14 skipping) conserve a few CEP192 functions that drive cell mitosis. Based on a previous study, U2OS cells with 5% CEP192 function can preserve the capacity to divide, but cell division and migration were partially blocked.[33] Thus, we propose here that the complete depletion of *CEP192* leads to the failure of cell division, indicating that CEP192 is indispensable in cell mitosis, and cells that conserve a few CEP192 functions can divide, but the division speed is slowed down.

Faithful segregation of homologous chromosome and sister chromatid is essential for generating functional spermatozoa.[34] Chromosome segregation errors during meiosis may result in spermatocyte apoptosis, aneuploidy, or tetraploidy and finally cause azoospermia or oligozoospermia and male infertility.[35] CEP192 works as a distinct scaffold to recruit PLK4 to centrosomes.[32] The loss of the CEP192-dependent interaction with PLK4 resulted in impaired centriole duplication, thus delaying cell proliferation.[32] *PLK4* is a known gene for a recessive disorder with partial MVA-related phenotypes.[15] In heterozygous status, *PLK4* variants cause male hypogonadism, azoospermia, and germ cell loss in humans and mice.[16–18] In this study,

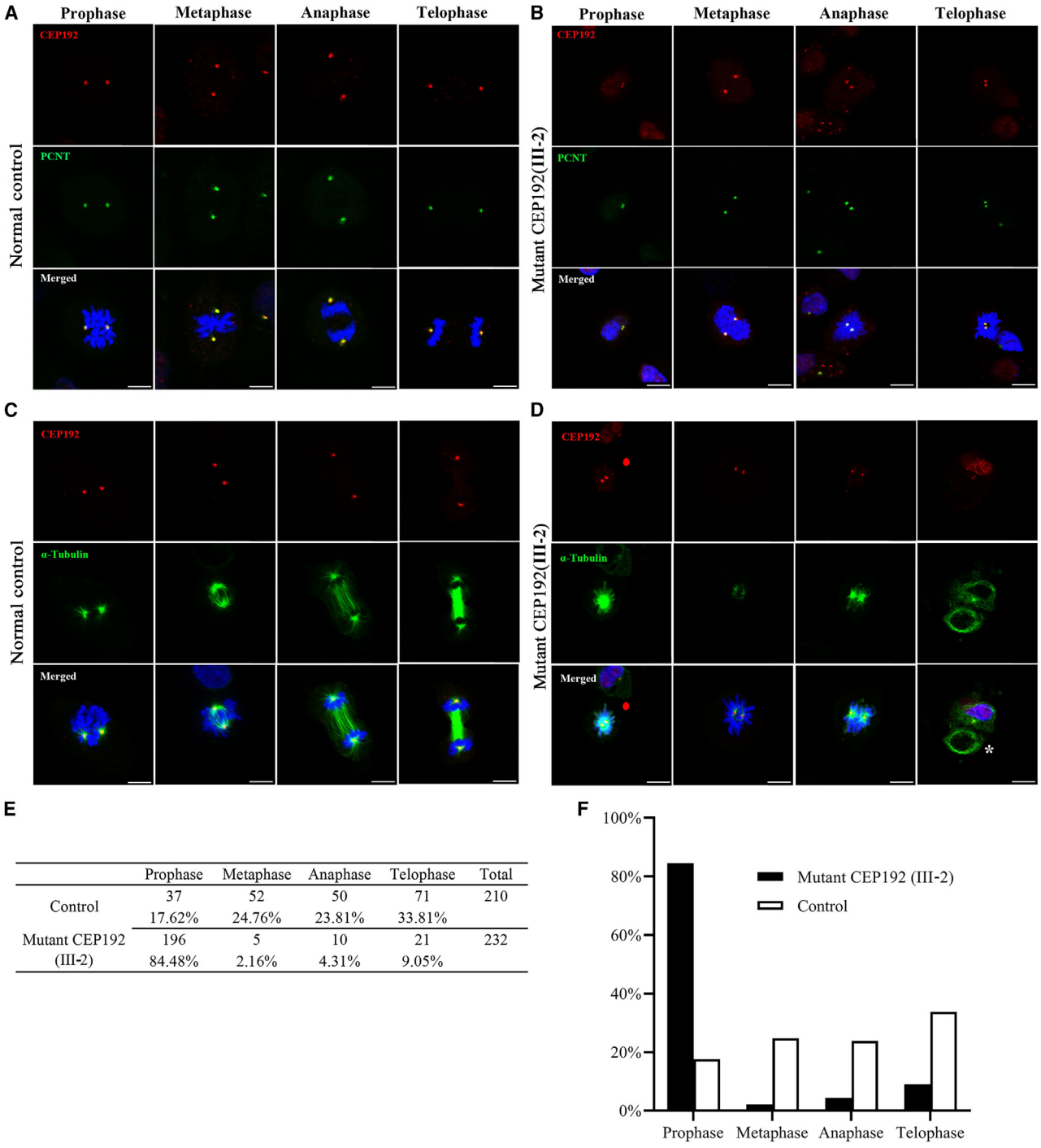

E

	Prophase	Metaphase	Anaphase	Telophase	Total
Control	37	52	50	71	210
	17.62%	24.76%	23.81%	33.81%	
Mutant CEP192 (III-2)	196	5	10	21	232
	84.48%	2.16%	4.31%	9.05%	

Figure 7. Mitosis defects and spindle formation abnormalities in cells from a patient with *CEP192* biallelic variants
(A and B) Immunofluorescence staining of epithelial cells from patient III-2 and a normal control using antibodies against CEP192 (red) and PCNT (green), and DAPI staining of DNA (blue). CEP192 proteins were co-localized with the centrosome in the different stages of mitosis in both cells from normal control and III-2. Scale bars, 7.5 μm.
(C and D) Immunofluorescence staining of epithelial cells from patient III-2 and a normal control using antibodies against CEP192 (red) and α-tubulin (green), and DAPI staining of DNA (blue). (C) Normal spindle formation at interphase, metaphase, anaphase, and telophase in epithelial cells were observed in the normal control. (D) Two centrosomes were not fully pulled apart per nucleus in epithelial cells from patients. Asterisks indicate the abnormal cells with unevenly distributed nuclei during cell division. Scale bars, 7.5 μm.
(E and F) Quantification of different stages in mitosis in epithelial cells from normal control and patient III-2.

both humans and mice with *CEP192* heterozygous variants showed susceptibility to infertility, probably because the mutant CEP192 fails to recruit PLK4.

This has some limitations. In this study, approximately 20%–30% of male mice with monoallelic *Cep192* defect ($Cep192^{+/-}$ or $Cep192^{+/M}$) were identified to be infertile,

from which small testes and histologic changes were observed. However, the remaining fertile *Cep192*$^{+/-}$ or *Cep192*$^{+/M}$ male mice exhibited seemingly normal testicular histology. Because of the embryonic lethality of the *Cep192*$^{-/-}$ or *Cep192*$^{M/M}$ mice, the effects in testicular change could not be studied in the homozygous state. Loss of germ cell and reduction in testis size present in some of the *Cep192* heterozygote mice may be a partial phenotype. The effect of a homozygous *Cep192* in the testis could be investigated using a conditional knockout model in our next work.

In conclusion, we identified biallelic pathogenic variants in *CEP192* as causing a rare disorder (MVA syndrome with tetraploidy) and monoallelic variants in causing a common disorder (male infertility). These findings expand our knowledge of the relationship between centrosome proteins and human disease and will allow the precise genetic diagnosis of MVA syndrome and male infertility.

Data and code availability

All CEP192 variants reported here have been deposited to ClinVar (accession numbers will be accessible to readers upon publication). Sequencing data are unavailable for sharing due to patient consent restrictions. For ES data from the CEP192 family F1, please contact the corresponding author Yongjia Yang. For detailed sequencing data or samples information from the 1,264-individual male infertility cohort, please contact corresponding author Yue-Qiou Tan.

Supplemental information

Supplemental information can be found online at https://doi.org/10.1016/j.xhgg.2023.100256.

Acknowledgments

We thank all family members who participated in this study. This study was supported by Natural Science Foundation of Hunan Province (2021JJ30390 to Y.Y. and 2023JJ30716 to W.-B.H.), National Natural Science Foundation of China (31501017 to Y.Y., 82101961 and 82171608 to Y.-Q.T., 82201773 to W.-B.H., and 81701437 to F.T.), the National Key Research and Development Program of China (2022YFC2702604 to Y.-Q.T.), and the Hunan Health Commission Research Fund (B2019019 to Y.Y. and B202301039323 to W.-B.H.). We thank the technician Yongzhong Guo for his contribution in animal feeding and maintenance.

Author contributions

The project was conceived and the experiments were planned by Y.Y. Experiments about sequencing of *CEP192* for 1,264 infertility males was planned by Y.-Q.T. The review of phenotypes and the sample collection for the index family were performed by Y.Y., J.G., M.T., L.Z., X.W., and H.W. The review of phenotypes and the sample collection for the 1,264 males with infertility were performed by W.-B.H., Y.-Q.T., C.T., L.-L.M., G.-X.L., and G.L. Comprehensive cytogenetic analysis was performed by Y.Y., J.G., F.S., M.T., L.Z., and C.T. Gene functional experiments were performed by L.D., Y.Y., W.-B.H., F.T., F.S., M.D., and S.Z. Bioinformatic analysis was performed by Y.Z., L.-L.M., Y.P., and Y.Y. Animal experiments were performed by J.G., W.-B.H., Z.L., F.T., W.L., and Y.Y.

Declaration of interests

The authors declare no competing interests.

Received: August 3, 2023
Accepted: November 15, 2023

Web resources

Huabiao-5000 human-exome-sequencing-data of general Chinese-Han-population, https://www.biosino.org/wepd
EAS_gnomAD, http://www.gnomad-sg.org/

References

1. Hanks, S., Coleman, K., Reid, S., Plaja, A., Firth, H., Fitzpatrick, D., Kidd, A., Méhes, K., Nash, R., Robin, N., et al. (2004). Constitutional aneuploidy and cancer predisposition caused by biallelic mutations in *BUB1B*. Nat. Genet. *36*, 1159–1161.
2. García-Castillo, H., Vásquez-Velásquez, A.I., Rivera, H., and Barros-Núñez, P. (2008). Clinical and genetic heterogeneity in patients with mosaic variegated aneuploidy: delineation of clinical subtypes. Am. J. Med. Genet. *146A*, 1687–1695.
3. Limwongse, C., Schwartz, S., Bocian, M., and Robin, N.H. (1999). Child with mosaic variegated aneuploidy and embryonal rhabdomyosarcoma. Am. J. Med. Genet. *82*, 20–24.
4. Plaja, A., Vendrell, T., Smeets, D., Sarret, E., Gili, T., Català, V., Mediano, C., and Scheres, J.M. (2001). Variegated aneuploidy related to premature centromere division (PCD) is expressed in vivo and is a cancer-prone disease. Am. J. Med. Genet. *98*, 216–223.
5. Lane, A.H., Aijaz, N., Galvin-Parton, P., Lanman, J., Mangano, R., and Wilson, T.A. (2002). Mosaic variegated aneuploidy with growth hormone deficiency and congenital heart defects. Am. J. Med. Genet. *110*, 273–277.
6. Snape, K., Hanks, S., Ruark, E., Barros-Núñez, P., Elliott, A., Murray, A., Lane, A.H., Shannon, N., Callier, P., Chitayat, D., et al. (2011). Mutations in *CEP57* cause mosaic variegated aneuploidy syndrome. Nat. Genet. *43*, 527–529.
7. Yost, S., de Wolf, B., Hanks, S., Zachariou, A., Marcozzi, C., Clarke, M., de Voer, R., Etemad, B., Uijttewaal, E., Ramsay, E., et al. (2017). Biallelic *TRIP13* mutations predispose to Wilms tumor and chromosome missegregation. Nat. Genet. *49*, 1148–1151.
8. Gerstung, M., Jolly, C., Leshchiner, I., Dentro, S.C., Gonzalez, S., Rosebrock, D., Mitchell, T.J., Rubanova, Y., Anur, P., Yu, K., et al. (2020). The evolutionary history of 2,658 cancers. Nature *578*, 122–128.
9. Shiono, H., Azumi, J., Fujiwara, M., Yamazaki, H., Kikuchi, K., Optiz, J.M., and Reynolds, J.F. (1988). Tetraploidy in a 15-month-old girl. Am. J. Med. Genet. *29*, 543–547.
10. Manic, G., Galluzzi, L., and Vitale, I. (2022 08). Catastrophic DNA replication in unscheduled tetraploid cells. Trends Genet. *38*, 787–788.

11. Margolis, R.L., Lohez, O.D., and Andreassen, P.R. (2003). G1 tetraploidy checkpoint and the suppression of tumorigenesis. J. Cell. Biochem. *88*, 673–683.
12. Prasad, K., Bloomfield, M., Levi, H., Keuper, K., Bernhard, S.V., Baudoin, N.C., Leor, G., Eliezer, Y., Giam, M., Wong, C.K., et al. (2022 05 03). Whole-Genome Duplication Shapes the Aneuploidy Landscape of Human Cancers. Cancer Res. *82*, 1736–1752.
13. Gabarrón, J., Jimenez, A., and Glover, G. (1986). Premature centromere division dominantly inherited in a subfertile family. Cytogenet. Genome Res. *43*, 69–71.
14. Chamla, Y. (1988). C-anaphases in lymphocyte cultures versus premature centromere division syndromes. Hum. Genet. *78*, 111–114.
15. Martin, C.-A., Ahmad, I., Klingseisen, A., Hussain, M.S., Bicknell, L.S., Leitch, A., Nürnberg, G., Toliat, M.R., Murray, J.E., Hunt, D., et al. (2014). Mutations in PLK4, encoding a master regulator of centriole biogenesis, cause microcephaly, growth failure and retinopathy. Nat. Genet. *46*, 1283–1292.
16. Miyamoto, T., Bando, Y., Koh, E., Tsujimura, A., Miyagawa, Y., Iijima, M., Namiki, M., Shiina, M., Ogata, K., Matsumoto, N., and Sengoku, K. (2016). A PLK4 mutation causing azoospermia in a man with Sertoli cell-only syndrome. Andrology *4*, 75–81.
17. Harris, R.M., Weiss, J., and Jameson, J.L. (2011). Male hypogonadism and germ cell loss caused by a mutation in Polo-like kinase 4. Endocrinology *152*, 3975–3985.
18. Tang, D., Li, K., Geng, H., Xu, C., Lv, M., Gao, Y., Wang, G., Yu, H., Shao, Z., Shen, Q., et al. (2022). Identification of deleterious variants in patients with male infertility due to idiopathic non-obstructive azoospermia. Reprod. Biol. Endocrinol. *20*, 63.
19. Wang, X., Tan, Y.-Q., and Liu, M.-F. (2022). Defective piRNA Processing and Azoospermia. N. Engl. J. Med. *386*, 1674–1675.
20. Li, L., Tan, Y.-Q., and Lu, L.-Y. (2022). Defective piRNA Processing and Azoospermia. N. Engl. J. Med. *386*, 1675–1676.
21. He, W.-B., Tan, C., Zhang, Y.-X., Meng, L.-L., Gong, F., Lu, G.-X., Lin, G., Du, J., and Tan, Y.-Q. (2021 03). Homozygous variants in SYCP2L cause premature ovarian insufficiency. J. Med. Genet. *58*, 168–172.
22. Yang, Y., Guo, J., Dai, L., Zhu, Y., Hu, H., Tan, L., Chen, W., Liang, D., He, J., Tu, M., et al. (2018 09). *XRCC2* mutation causes meiotic arrest, azoospermia and infertility. J. Med. Genet. *55*, 628–636.
23. Zheng, Y., Peng, Y., Zhang, S., Zhao, H., Chen, W., Yang, Y., Hu, Z., Yin, Q., and Peng, Y. (2022). Case Report: MYO5B Homozygous Variant c.2090+3A>T Causes Intron Retention Related to Chronic Cholestasis and Diarrhea. Front. Genet. *13*, 872836.
24. Lyu, Q.F., Deng, L., Xue, S.G., Cao, S.F., Liu, X.Y., Jin, W., Wu, L., and Kuang, Y. (2010). New technique for mouse oocyte injection via a modified holding pipette. Reprod. Biomed. Online *21*, 663–666.
25. Jiang, S., Peng, X., Gong, F., Huang, C., Peng, Y., Long, X., Lin, G., and Zhu, W. (2020). The role of total chromosomal disomy in human spermatozoa as a predictor of the outcome of preimplantation genetic screening. Fertil. Steril. *113*, 1196–1204.e1.
26. van Breugel, M., Rosa E Silva, I., and Andreeva, A. (2022 04 05). Structural validation and assessment of AlphaFold2 predictions for centrosomal and centriolar proteins and their complexes. Commun. Biol. *5*, 312.
27. Zhu, F., Lawo, S., Bird, A., Pinchev, D., Ralph, A., Richter, C., Müller-Reichert, T., Kittler, R., Hyman, A.A., and Pelletier, L. (2008). The mammalian SPD-2 ortholog Cep192 regulates centrosome biogenesis. Curr. Biol. *18*, 136–141.
28. Human Splicing Finder-Version 3.1. http://www.umd.be/HSF3/HSF.shtml.
29. Jaganathan, K., Kyriazopoulou Panagiotopoulou, S., McRae, J.F., Darbandi, S.F., Knowles, D., Li, Y.I., Kosmicki, J.A., Arbelaez, J., Cui, W., Schwartz, G.B., et al. (2019). Predicting Splicing from Primary Sequence with Deep Learning. Cell *176*, 535–548.e24.
30. Gomez-Ferreria MA, R.U., Buster, D.W., Chanda, S.K., Caldwell, J.S., Rines, D.R., and Sharp, D.J. (2007). Human Cep192 is required for mitotic centrosome and spindle assembly. Curr. Biol. *17*, 7.
31. Joukov, V., Walter, J.C., and De Nicolo, A. (2014). The Cep192-organized aurora A-Plk1 cascade is essential for centrosome cycle and bipolar spindle assembly. Mol. Cell *55*, 578–591.
32. Sonnen, K.F., Gabryjonczyk, A.M., Anselm, E., Stierhof, Y.D., and Nigg, E.A. (2013). Human Cep192 and Cep152 cooperate in Plk4 recruitment and centriole duplication. J. Cell Sci. *126* (Pt 14), 3223–3233.
33. O'Rourke, B.P., Gomez-Ferreria, M.A., Berk, R.H., Hackl, A.M.U., Nicholas, M.P., O'Rourke, S.C., Pelletier, L., and Sharp, D.J. (2014). Cep192 controls the balance of centrosome and non-centrosomal microtubules during interphase. PLoS One *9*, e101001.
34. Xie, C., Wang, W., Tu, C., Meng, L., Lu, G., Lin, G., Lu, L.-Y., and Tan, Y.-Q. (2022). Meiotic recombination: insights into its mechanisms and its role in human reproduction with a special focus on non-obstructive azoospermia. Hum. Reprod. Update *28*, 763–797.
35. Handel, M.A., and Schimenti, J.C. (2010). Genetics of mammalian meiosis: regulation, dynamics and impact on fertility. Nat. Rev. Genet. *11*, 124–136.